Philip S. Marcus
Steven A. Orszag
Anthony T. Patera
Department of Mathematics
Massachusetts Institute of Technology
Cambridge, MA 02139 USA

SIMULATION OF CYLINDRICAL COUETTE FLOW

We have developed, tested, and implemented a numerical code for calculating the viscous, three dimensional flow between two differentially rotating cylinders (cylindrical Couette flow). In this paper we describe the methods that we have used to apply efficiently pseudo-spectral techniques to a complicated (i.e. non-Cartesian) geometry with real (i.e. viscous, no-slip) boundaries and the tests that we have used to determine the accuracy of our code.

I. OBSERVED STATES OF COUETTE FLOW

When the inner cylinder is rotating and the outer cylinder is held stationary, four non-chaotic flows have been observed experimentally. We define the Reynolds number as $RE = \Omega R_1 (R_2 - R_1)/\nu$ where ν is the viscosity, Ω is the angular velocity of the inner cylinder, and R_1 and R_2 are the radii of the inner and outer cylinders. We also define the radius ratio ξ to be R_1/R_2. For a given geometry, as the Reynolds number is increased to RE_{crit}, the stable flow changes from its laminar profile to N axisymmetric Taylor vortices stacked on top of each other. Near the endplates the vortices disappear. The upper surface boundary condition (rigid or free) strongly influences whether N is even or odd. A rigid upper surface tends to make N even. The Couette system selects the number N so that the axial wavelength of the cells, λ, is of order twice the radial gap separation (which is nearly the critical axial wavelength for the onset of the Taylor vortices). The number N is not unique for a fixed Reynolds number and geometry and is determined by the past history of the system. As the Reynolds number is increased further, azimuthal traveling waves [proportional to $\exp(im_1\theta)$] form on the vortices. Each state in this regime can be identified by N and m_1. The waves travel with a speed c_1. If this state is observed in the proper rotating frame, it appears as a steady-state. Although the speed c_1 depends on the radii of the inner and outer cylinders, it appears to be almost independent of m_1. For Reynolds numbers near critical, the wave speed is a strong function of RE, but for RE greater than ~6 times the critical value, the wave speed approaches a constant value. The wave speed is also a function of the axial wavelength. This non-axisymmetric, steady (in the proper rotating frame) flow becomes unstable as the Reynolds number is increased further and two traveling waves appear. The second traveling wave has azimuthal number m_2 and phase speed c_2. The second wave speed depends upon the radius ratio and weakly depends on N, m_1, m_2, and the Reynolds number. When the flow has one or two traveling waves, the states are meta-stable and the Reynolds number alone does not determine uniquely which particular state the flow will be. The numbers (N,m_1,m_2) that characterize the flow are not unique functions of the Reynolds number but depend upon the past history of the flow. The flow with two traveling waves does not appear as a steady state to any observer. When the Reynolds number is greater than a second critical value, the time spectrum of the flow develops a broad component centered around a frequency f_b. In this case, the motions are aperiodic (weakly chaotic). There is an increase in the amount of small scale structure visible in the flow as the Reynolds number is increased further. The azimuthal traveling waves eventually disappear but the Taylor vortex cells persist to the highest values of Reynolds number examined.

II. EQUATIONS AND BOUNDARY CONDITIONS

Our primary motivation for writing an initial-value code rather than a steady-state solver is that we are interested in computing the transitions among

the four non-chaotic flows. One of the flows is quasi-periodic and not a steady-state. The initial-value equation that we solve is the Navier-Stokes equation in cylindrical coordinates with the boundary conditions that the radial and axial components of the velocity at the radial boundaries vanish and that the azimuthal components of the velocity match the cylinder rotation speed, Ω, at the walls. We assume periodicity in the axial direction and require that the velocity be divergence-free.

In a reference frame rotating with angular velocity C with respect to the inertial frame, the Navier-Stokes equation is

$$\frac{\partial v_c}{\partial t} = (v_c + v_{LAM} - C\, r\hat{e}_\theta) \times (\omega_c + \omega_{LAM}) + RE^{-1}\nabla^2 v_c - \nabla P_c \qquad (1)$$

where the velocity seen by an observer in the inertial frame, $\hat{v}$, is

$$\hat{v}(r,\theta,z,t) \equiv v_c(r,\theta+ct,z,t) + v_{LAM}(r) \qquad (2)$$

where v_{LAM} is the laminar velocity of Couette flow (as seen in the inertial frame)

$$v_{LAM}(r) = \frac{\xi}{1-\xi^2}\left[\frac{1}{r(1-\xi)} - r(1-\xi)\right]\hat{e}_\theta \qquad (3)$$

where ω_{LAM} is the vorticity of the laminar flow

$$\omega_{LAM} = -2\xi/(1+\xi)\ \hat{e}_z \qquad (4)$$

and where ω_c is the relative vorticity

$$\omega_c(r,\theta,z,t) \equiv \nabla \times v_c(r,\theta,z,t). \qquad (5)$$

We use the relative velocity $v_c(r,\theta,z,t)$ as our dependent variable rather than the full velocity because $v_c(r,\theta,z,t)$ obeys the homogeneous boundary condition:

$$v_c(r,\theta,z,t) = 0 \quad \text{at the radial bounaries.} \qquad (6)$$

In equation (1) the velocity is in units of ΩR_1 and the length is in units of (R_2-R_1). Our code is designed so that the speed of the rotating frame of the observer, C, can be easily changed at any timestep (in fact we generally automatically update C so that one of the two traveling waves appears steady). Equation (1) is solved spectrally and we adopt the notation that each variable $Q(r,\theta,z,t)$ is written as the spectral sum:

$$Q(r,\theta,z,t) = \sum_m \sum_k \tilde{Q}(r,m,k,t)\exp[i(m\theta+2\pi kz/\lambda)] \qquad (7)$$

Note that $\hat{e}_r \cdot v_c(r,m=0,k=0,t)$ must always be identically equal to zero.

The radial dependence of each quantity is evaluated at the Chebyshev collocation points. Radial derivatives are found by fast-Fourier transforming into Chebyshev space, taking the spectral derivative, and inverse transforming back into physical radial space. Azimuthal and axial derivatives are evaluated spectrally. The nonlinear terms are computed by transforming into axial and azimuthal physical space, multiplying the values at the collocation points, and then inverse transforming. We do not remove aliasing errors.

III. THE TIME-SPLITTING STEPS

The nonlinear terms are computed in rotation form using a second-order Adams-Bashforth method. The velocity at the end of the nonlinear fractional step that goes from timestep N to timestep N+1 is:

$$v^{N+1/3}(r,\theta,z,t) = \frac{\Delta t}{2}[3(v_c^N + v_{LAM} - C\, r\hat{e}_\theta) \times (\omega_c^N + \omega_{LAM}) + v_c^N - (v_c^{N-1} + v_{LAM} - C\, r\hat{e}_\theta) \times (\omega_c^{N-1} + \omega_{LAM})] \quad (8)$$

(For the remainder of this section, we assume that the angular speed of the observer, C, is zero to simplify the notation and the presentation of the equations. We omit the subscript, C, from the velocity.) The stability of the explicit nonlinear step in equation (8) is governed by the Courant condition. We can modify equation (8) to allow bigger timesteps by observing that even in a rotating frame, the largest velocity component is the z-independent, axisymmetric (m=0,k=0) component of the azimuthal velocity. In cylindrical Couette flow the mean azimuthal velocity is analogous to the mean temperature gradient in convection; it drives the advective instability and has a profile that is modified by order unity due to the nonlinear interactions. Like the mean temperature gradient, the mean velocity becomes modified so that in the interior of the flow the mean profile is nearly neutrally stable. Typically, $|\tilde{v}'| < 50.0\ |\tilde{v}_\theta(r,0,0,t)|$ where $\tilde{v}' \equiv \tilde{v} - \tilde{v}_\theta(r,0,0,t)\,\hat{e}_\theta$. We therefore treat the nonlinear contribution of $\tilde{v}_\theta(r,0,0,t)$ and $\tilde{\omega}_\theta(r,0,0,t)$ implicitly.

Adding the gradient of the pressure to $v^{N+1/3}$ makes the velocity divergence-free at the end of the next fractional step:

$$v^{N+2/3} = v^{N+1/3} - \nabla\Pi^{N+1} \quad (9)$$

The pressure head, Π^{N+1}, is computed by requiring that $v^{N+2/3}$ be divergence-free at the interior points. At the radial boundaries we require that $\partial v_r^{N+1}/\partial r = 0$. This last condition is equivalent to requiring that $\nabla\cdot v^{N+1} = 0$ at the radial boundaries. (We do not impose the boundary condition that $\partial v_r^{N+2/3}/\partial r = 0$ because we have found that it leads to a slow instability.) Since v^{N+1} is unknown during this fractional step, we write

$$\Pi^{N+1} = \Pi_{invis}^{N+1} + \Phi^{N+1} \quad (10)$$

where

$$\nabla^2\Pi^{N+1} = \nabla\cdot v^{N+1/3} \quad \text{in the fluid interior} \quad (11)$$

$$\nabla^2\Phi^{N+1} = 0 \quad \text{in the fluid interior} \quad (12)$$

and where Π_{invis}^{N+1} satisfies the inviscid boundary condition for the pressure

$$\frac{\partial\Pi_{invis}^{N+1}}{\partial r} = \hat{e}_r \cdot v^{N+1/3} \quad \text{at the boundaries} \quad (13)$$

The viscous step is the final fractional step and gives v^{N+1}:

$$v^{N+1} = v^{N+2/3} + \frac{\Delta t}{2RE}\nabla^2(v^N + v^{N+1}) \quad \text{in the fluid interior} \quad (14)$$

The operator $(1 - \frac{\Delta t}{2RE}\nabla^2)$ is inverted by requiring $v_r = v_\theta = v_z = 0$ at the radial boundaries. The Greens function, Φ^{N+1}, is evaluated at the end of the viscous step. It is computed by evaluating a (diagonal) capacitance matrix once in a pre-processing stage and inverting the capacitance matrix after each viscous step.

Using the Greens function with the fractional step method produces a global temporal error of $\mathcal{O}(\Delta t^2)$. Instead of using Greens functions we can reduce the time-splitting error by solving the pressure equation with the inviscid boundary condition and using a Richardson extrapolation. For this particular geometry we have found that the use of Greens functions require no more

storage than a Richardson extrapolation, but uses significantly less computing time. Furthermore, the Richardson extrapolation error is $\mathcal{O}(\Delta t^{3/2})$ in the velocity and larger than $\mathcal{O}(\Delta t)^{3/2}$ for the radial derivatives of v_r at the boundary. In particular, the error in $\frac{\partial^2 v_r}{\partial r^2}$ using a Richardson extrapolation remains order unity.

IV. RESULTS

In addition to an initial-value code, we have written an eigenvalue code that solves the linearized sixth-order Navier-Stokes equation without the use of fractional steps. (The divergence of the velocity is everywhere zero including the boundaries). We have compared the linear eigenvalues (both the real and imaginary parts) computed from our linear eigenvalue-solver to the growth rates and velocities computed from the initial-value solver. For large Reynolds numbers, the errors in the growth rates and velocities from the initial-value solver decrease as Δt^2 (until the timestep is so small that truncation errors begin to dominate). The decrease confirms that the code is second-order accurate in time and shows that in the linear equations the splitting error is small. For the smallest timestep the errors in the growth rate and velocity are one part in 10^6 . We have also compared these eigenvalues to those calculated by Chandrasekhar (1961) for axisymmetric modes in a viscous fluid with ξ =0.5 and to those of Kreuger, Gross, and DiPrima (1966) for non-axisymmetric, viscous flows in a thin gap with ξ =0.95. We agree with these eigenvalues within one part in 10^4 .

We have several checks of consistency within our code. When a solution settles down to a quasi-periodic, periodic, or steady state, we calculate the divergence of the velocity. The divergence is a good measure of the time splitting error. We have found that for all modes (k,m) $(\nabla\cdot\tilde{v})/|\tilde{v}|\ \min(k,m/r)$ is less than 10^{-6} not only at the fluid interior but also at the radial boundaries. For flows with one traveling wave, we also compute the curl of $(v\times\omega+RE^{-1}\nabla^2 v)$ which should be zero (when observed in the rotating frame of the traveling wave). We find that $\nabla\times(v\times\omega + RE^{-1}\nabla^2 v)$ (in units of the average enstrophy) is of order 10^{-6}. In the steady state the rate of angular momentum flux in the radial direction

$$F = \frac{2\pi}{RE} r^3 \frac{\partial r\tilde{v}_\theta(r,0,0,t)}{\partial r} - \int r^2 v_r v_z d\theta dz / \int dz \qquad (15)$$

should be independent of radius and equal to the torque at the boundary. We find that the fractional variation in flux over the entire radius is about 0.003%. We have also solved the same initial-value problem (i.e. the same radius ratio and Reynolds number) several times while forcing the code to compute the solutions in different rotating reference frames. In one rotating frame the flow (with one traveling wave) appears as a steady-state but in the other frames it is periodic in time. Comparison of these solutions allows us to measure the temporal accuracy of the time-splitting when the nonlinear terms are large. We find that even for large nonlinear terms, the time stepping error remains small.

We have also measured the initial angular momentum of the flow. The initial angular momentum plus the temporally integrated torque should be equal to the angular momentum of the fluid in its final state. This type of consistency measure very accurately tests the torque and the structure of the solution near the boundary. The fractional difference between the actual angular momentum and that predicted by integrating the torques for ~ 4 rotation periods of the inner cylinder is of order 10^4 .

We have compared our numerically calculated torques with those measured experimentally by Donnelly and Simon (1960) for axisymmetric Taylor vortex flow with a radius ratio of ξ =0.5. and for Reynolds numbers up to 4 times the critical value. Our agreement is within experimental error. One difficulty in comparing the torques with experiments is that there is a slight dependence of torque on the axial wavelength. The torque measurements of Donnelly and Simon (and almost all other experimentalists) are done with opaque cylinders so that the axial

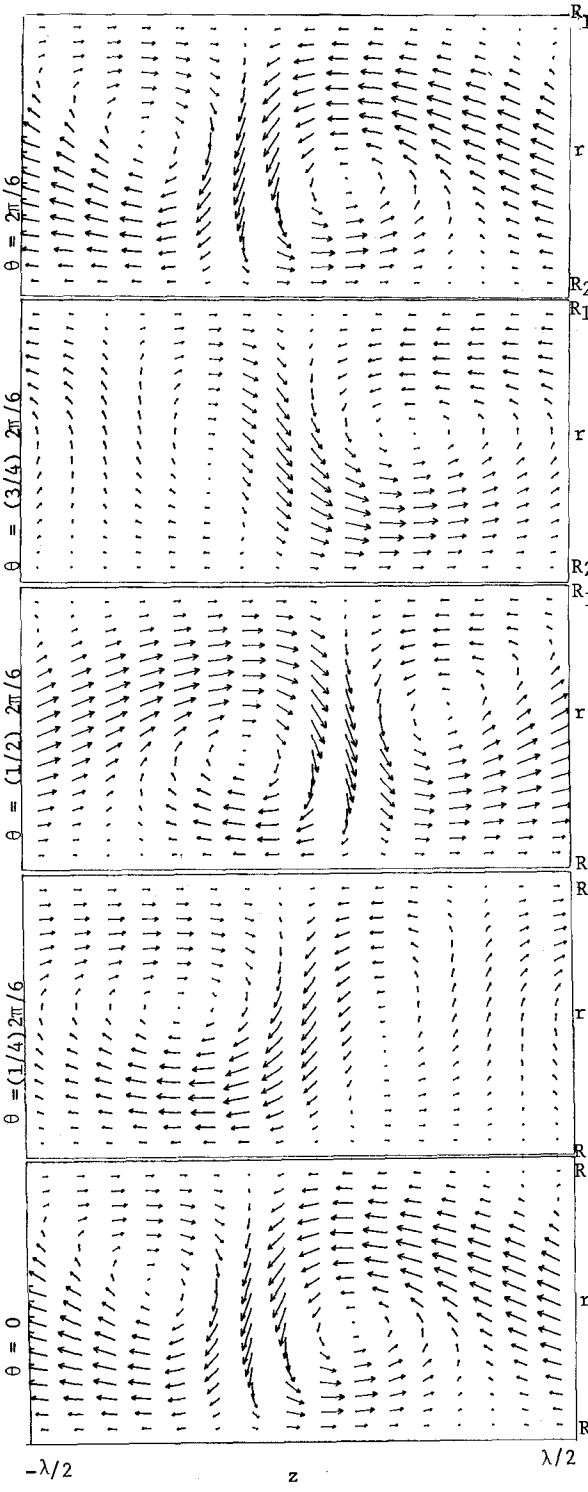

wavenumber (and often the azimuthal wavenumber) is not known and must be assumed. We have also found good agreement between our torques computed from an initial-value solver and those torques computed by Meyer-Spasche and Keller (1980)using a steady-state solver.

The most severe test that we have performed is the calculation of the wave speeds. We have found that at large Reynolds number (10 times RE_{crit}) where the wave speed is insensitive to the exact value of the Reynolds number, one can be somewhat cavalier with the treatment of the boundary conditions and obtain the correct result for the wave speed. At small values of the Reynolds number (2 times RE_{crit}) , the boundaries must be treated very carefully. Table 1 shows the experimentally measured values of the wave speed c_1, for RE=459.8 ≈3.96 times RE_{crit} with radius ratio ξ= 0.875 and m = 6 for the two extreme values of the axial wavelength (i.e. flows whose axial wavelengths are not between these two numbers are unstable or nearly unstable and difficult to maintain experimentally). Table 1 also includes the experimental value of c_1 for RE = 230.2 ≈2.00 times RE_{crit} with ξ = 0.868 and m = 6 for two extreme values of the axial wavelength. Included in the table are our numerical values computed with 33 radial collocation points, 32 axial collocation points per Taylor cell pair, and 16 aximuthal points per 2π/6 radians. Our calculated wave speeds agree with the laboratory measurements within the experimental uncertainty. We have agreement to 3 significant digits in the wave speed. The experimentally measured values of the wave speed are only accurate to 1% due to the uncertainties in the viscosity (or Reynolds number) while the experiments are being performed. The experimental measurements

of c_1 presented here were done by King and Swinney (1982). We have found similar agreement between our numerically computed wave speeds c_1 and c_2 and the experiments for flows with two traveling waves at larger ($RE \approx 10\ RE_{crit}$) Reynolds numbers.

TABLE 1

RE_{crit}	RE/RE_{crit}	λ	c_1 lab	c_2 numerical	ξ
115.1	2.05	3.00	0.365	0.3647	0.868
115.1	2.00	2.14	0.403	0.4028	0.868
116.1	3.96	2.32	0.359	0.3596	0.875
116.1	3.96	3.90	0.339	0.3397	0.875

wave speeds for m=6 traveling wave

All four of the flows presented in Table 1 have a symmetry in addition to being 6-fold symmetric about the axis of rotation. They also have the symmetry $v_r(r,\theta,z) = v_r(r,\theta+\frac{2\pi}{12} - z)$, $v_\theta(r,\theta,z) = v_\theta(r,\theta+\frac{2\pi}{12},z)$, $v_z(r,\theta,z) = -v_z(r,\theta+\frac{2}{12}-z)$ We show this symmetry by plotting the azimuthal modulation of a pair of Taylor cells. Figure 1 shows the v_z and v_r components of the velocity in the (z-r) plane for five different values of θ.

This work was supported by the Office of Naval Research Contract#N00014-82-C-0451, a National Science Foundation Fellowship #SPI-8009181, and the Air Force Office of Scientific Research under Grant # 77-3405.

REFERENCES

Chandrasekhar, S., (1960), Hydrodynamic and Hydromagnetic Stability, Oxford University Press.
Donnelly, R. J., & Simon, N.J., 1960, J.F.M., 7, 401.
King, G., & Swinney, H.L., 1982, private communication.
Kreuger, E. R., Gross, A., & DiPrima, R.C., 1966, J.F.M., 24,521.
Meyer-Spasche, R., & Keller, H. B., 1980 J. Comp. Phys., 35, 100.